frontiers in Physics

ORIGINAL RESEARCH
published: 21 February 2022
doi: 10.3389/fphy.2022.843852

All-Optical Polarization Manipulation Through Orbital Polarization Holography

*Ziyao Lyu and Changshun Wang**

State Key Laboratory of Advanced Optical Communication Systems and Networks, School of Physics and Astronomy, Shanghai Jiao Tong University, Shanghai, China

Spin-orbital optical phenomena are closely related with light-matter interactions and have been of great interest in the last few years. Here, the effect of optical orbital angular momentum (OAM) on polarized waves carrying spin angular momentum (SAM) has been investigated experimentally by means of orbital polarization holography and analyzed with Jones matrices theoretically. We report that all-optical OAM-to-polarization manipulation can be realized with a controllable holographic grating recorded through the interference of orthogonally polarized beams in various helical modes in a kind of photo-alignment supermolecular liquid-crystalline films. The polarization states of diffraction beams can be controlled through adjusting the spatial degree of freedom of the recording light field. The OAM-controlled polarization manipulation is discussed in terms of Jones matrices and photoinduced birefringence. Because of the realization of OAM-to-SAM conversion, this work may find applications in a variety of devices.

Keywords: Jones matrix, polarization control, photoinduced birefringence, spin-orbit interaction, holography

OPEN ACCESS

Edited by:
Tingchao He,
Shenzhen University, China

Reviewed by:
Wenbo Hu,
Northwestern Polytechnical University, China
Jianming Wen,
Kennesaw State University, United States

****Correspondence:***
Changshun Wang
cswang@sjtu.edu.cn

Specialty section:
This article was submitted to Physical Chemistry and Chemical Physics, a section of the journal Frontiers in Physics

Received: *27 December 2021*
Accepted: *31 January 2022*
Published: *21 February 2022*

Citation:
Lyu Z and Wang C (2022) All-Optical Polarization Manipulation Through Orbital Polarization Holography. Front. Phys. 10:843852. doi: 10.3389/fphy.2022.843852

INTRODUCTION

Transfer of optical angular momentum (AM) has been proposed in the last few decades as an effective tool to achieve optical manipulation, quantum communication and so on [1, 2]. Generally, there are two kinds of AM carried by light, spin AM (SAM) and orbital AM (OAM). SAM is inherent in light beams with circular or elliptical polarization states and depends on the field vector rotations that take place in every point of the beam cross-section [3]. When the light is right- or left-handed circularly polarized (RCP or LCP), SAM equals $\pm\hbar$ per photon, respectively [4]. Polarization is a fundamental property of electromagnetic fields and the polarization state of light has substantial influence in an increasing number of optical experiments and theoretical models [5]. In the field of optics, the polarization state of light can significantly affect the propagation of many fully or partially coherent paraxial light fields. Moreover, optical communications, laser science, microscopy and metrology demand control of light polarization [6–8]. On the other hand, optical vortex has become increasingly important recently [9, 10]. A vortex beam, with the spiral phase of $\exp(il\phi)$ with l being the topological charge (TC) and ϕ being the azimuth angle, possesses intrinsic OAM [11]. OAM can be added to a Gaussian beam through a spiral phase plate (SPP) which is typically a high refractive index substrate that is shaped into the spiral phase ramp [3, 12]. The incident Gaussian beam is not deviated in direction and directly converted to a vortex beam. Like polarization, OAM of light provides the spatial degree of freedom, which can be of great benefit in many fields, such as holography [13, 14].

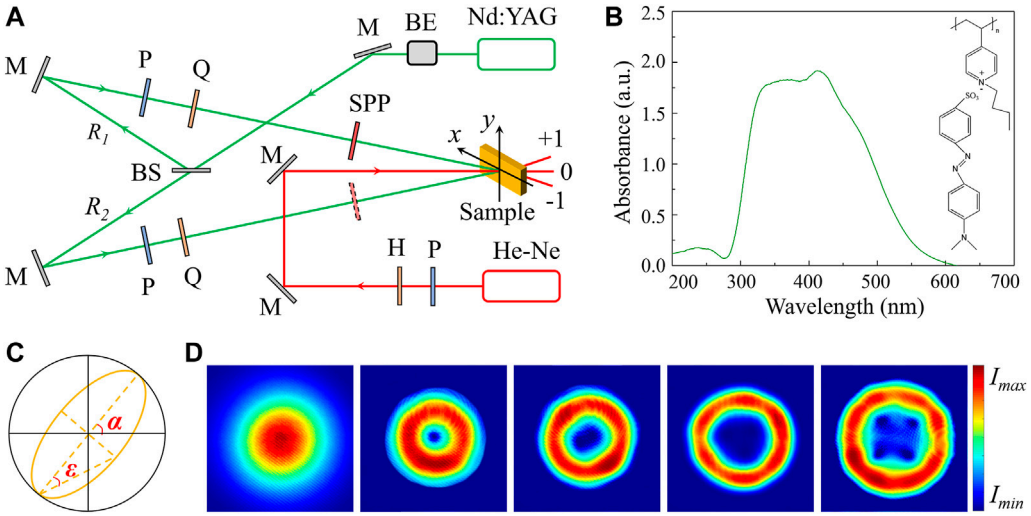

FIGURE 1 | (A) Schematic setup of orbital polarization holography. BE, beam expander; M, mirror; BS, beam splitter; P, polarizer; Q, quarter-wave plate; H, half-wave plate; SPP, spiral phase plate. **(B)** Absorption spectrum and molecular structure of the photo-alignment liquid-crystalline film. **(C)** Diagram of the polarization ellipse with α being the azimuth and ε being the ellipticity. **(D)** Spatial intensity distribution of the recording light with TC of 0, 1, 2, 3 and 4 (from left to right) measured by CCD.

There are two important kinds of holography, namely polarization holography and OAM holography. In terms of polarization holography, the recording beams can be orthogonally circularly polarized and the interference field possesses constant light intensity with periodically distributed polarization in space [15–17]. Then, the polarization pattern is recorded and stored in photo-alignment materials. Polarization holography is an attractive technique for its unique capacity of recording intensity, phase, and polarization of a wave simultaneously along with the function of polarization modulation [18]. With the development of optical vortex, OAM holography also emerges as an effective method for data storage and information processing [19, 20]. Recently, there has been enormous interest in spin-orbit interactions of light [21, 22]. These are striking optical phenomena in which the polarization and spatial degrees of freedom of light affect each other. Traditionally, spin-orbit interactions in optics usually describe an influence of the polarization degree of freedom of light on its spatial properties [23–26]. However, the reverse process, i.e., OAM controls SAM, still needs more research.

In this article, polarization manipulation enabled by the spatial degree of freedom of light has been investigated experimentally by means of angular momentum holography, where SAM-OAM coupling takes place within the optical interference field during the process of light-matter interactions, resulting in the formation of a kind of photoinduced periodic birefringence structure in photo-alignment liquid crystals, namely the orbital polarization holographic grating (OPHG). We report that the polarization states of diffraction light from the recorded OPHG can be controlled through the spatial degree of freedom of recording light. The mechanism of OAM-to-SAM manipulation and the diffraction properties of OPHG are analyzed in terms of Jones matrices, and the photoinduced birefringence generated through SAM-OAM coupling as well as the transmission matrix of OPHG are calculated in order to interpret the effect of OAM-controlled polarization manipulation.

MATERIALS AND METHODS

Sample Preparation

A kind of photo-alignment material through ionic self-assembly of poly ionic liquid and methyl orange dyes is chosen as the sample in this experiment because of the properties of strong photoinduced anisotropy and good thermal stability [27]. The charged polymer poly (1-butyl-vinylpyridinium bromide) is selected as the main chain and the methyl orange dye is selected as the building unit, as shown in **Figure 1B**. For the preparation of ionic self-assembly complex, 2 mg/ml poly ionic liquid aqueous solution is added to methyl orange aqueous solution at the molar charge ratio of 1:1. The precipitated complex is filtrated and washed several times with doubly distilled water, then dried in vacuum at 60°C for 12 h. The thickness of the liquid-crystalline film is 2 μm.

Experimental Setup

The experimental setup is depicted in **Figure 1A**. A 532 nm beam with the power density of 250 mW/cm^2 from a Nd:YAG laser is selected as the pump light, according to the absorption spectrum of the sample in **Figure 1B**. The pump light passes through a beam expander and is divided by a 50:50 beam splitter. The two recording beams, marked as R_1 and R_2, are controlled to keep left- and right-handed circularly polarized, respectively. Then, an extra spiral phase is added to R_1 or R_2 in order to generate a vortex recording beam. The two recording beams interfere at the surface of the sample at an angle of 4° and the recording time is 100 s. The diffraction property of the recorded OPHGs is investigated through a 633 nm probe light with the power

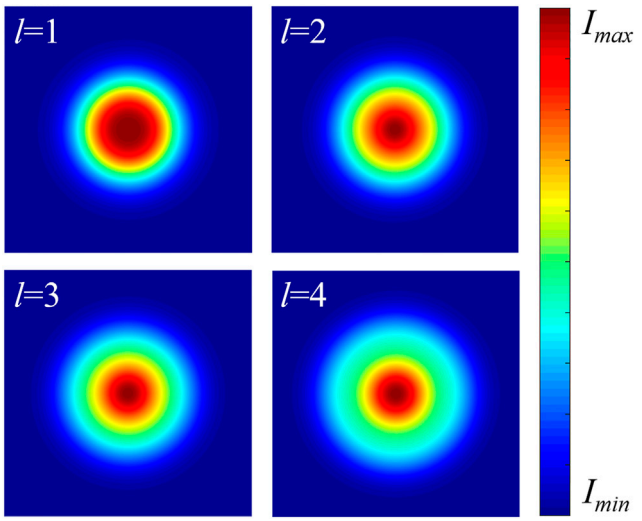

FIGURE 2 | Light intensity distribution within the orbital polarization holographic recording field when the value of TC increases from 1 to 4. The total intensities of the interference fields are the sum of the intensities of the two recording beams without interference fringes.

density of 150 mW/cm^2 from a He-Ne laser. The diameters of the two recording beams are both 1.6 mm and the size of the probe light is controlled to be the same with that of the Gaussian recording beam in order to illuminate the whole OPHG. The spatial intensity distribution and polarization state of light are measured with CCD (CINOGY, CinCam-1201) and free-space polarimeter (THORLABS, PAX5710VIS-T), respectively. As shown in **Figure 1C**, the polarization state detected with the polarimeter is presented as a polarization ellipse that can be described with two parameters, azimuth α and ellipticity ε, related to Stokes parameters. In terms of the spatial intensity distribution of the vortex recording light in **Figure 1D**, there is no change for the laser spot when the polarization state varies from LCP to RCP under all four TC conditions. The polarization state also keeps constant with TC being manipulated [28]. For ease of description, the recorded OPHG is expressed as OPHG ($l_{Ri} = n$) with R_i being the vortex recording light and n being the value of TC. The distributions of light intensities under four TC conditions are presented in **Figure 2**. Because the two recording beams are orthogonally polarized, the total light intensities of the interference fields are the sum of the intensities of R_1 and R_2 without interference fringes and only the polarization state changes periodically in space [29].

RESULTS

Orbital-Dependent Polarization Manipulation

First of all, OPHG ($l_{R1} = 1$) is recorded. The probe light is linearly polarized and the polarization direction is rotated counterclockwise through a half-wave plate, i.e., α_p is modulated from −90° to 90°. The polarization state of probe light changes in the same way in subsequent experiments. As OAM is added to the holographic recording field, the polarization state of the zeroth-order diffraction light is controlled to be left-handed elliptically polarized, as reported on the Poincaré sphere in **Figure 3A**, which is different from the convention holographic grating whose polarization state is not modulated. The zeroth diffraction order of OPHG ($l_{R1} = 1$) is regulated to possess SAM and the ellipticity almost remains constant ($-21.75° \leq \varepsilon \leq -19.48°$) as the polarization direction of the probe light rotates in a circle. Then, we remove the SPP and record another polarization holographic grating (PHG) as a comparison and the experimental results are presented in **Figure 3B**. According to **Figures 3A,B**, the polarization state of the zeroth-order diffraction light from PHG keeps the same with that of incident light, and thus SAM manipulation is attributed to the spatial degree of freedom of recording light through orbital polarization holography. Besides, **Figure 3C** presents that, for OPHG ($l_{R1} = 1$), the azimuth of the elliptically polarized zeroth-order diffraction light is not regulated by OAM and keeps the same with that of the probe light.

As the probe light illuminates the recorded OPHG ($l_{R1} = 1$), the ± 1st diffraction orders with the diffraction efficiency of 9.83% are detected and the polarization states are presented in **Figure 4**. It can be noticed that both of the ± 1st order diffraction beams are modulated to be elliptically polarized by OPHG ($l_{R1} = 1$) and the value of ellipticity varies with the polarization direction of probe light. The diffraction property of the recorded OPHG is also different from that of PHG under the same experimental conditions [17]. As OAM is added to the holographic interference field, the polarization state of diffraction light from OPHG ($l_{R1} = 1$) can be modulated and the modulation depth is dependent on the spatial degree of freedom of recording light.

Then, OPHG ($l_{R1} = 1$) is erased through the heating method. The sample is heated up to 60°C, in which thermally randomizing the molecular orientations occurs. This writing-erasing cycle could be repeated over 100 times on the same spot of the film without fatigue. Another OPHG ($l_{R2} = 1$) is recorded and the diffraction efficiency of the ± 1st diffraction order is 12.82%. The polarization states of the ± 1st order diffraction light from OPHG ($l_{R2} = 1$) are presented in **Figure 4**. The −1st order diffraction light is modulated to be right-handed elliptically polarized while the other one becomes left-handed elliptically polarized. The experimental results indicate that polarization manipulation enabled by the spatial degree of freedom of light still exists when the handedness of SAM within the orbital polarization holographic recording field is reversed. However, the polarization changing behaviors of the 1st order diffraction light are not the same with those of OPHG ($l_{R1} = 1$). Firstly, the ellipticity of the same diffraction order from the two OPHGs is investigated. In **Figure 4A**, it can be noticed that the changing behaviors of ellipticity of the -1st order diffraction beams from OPHGs ($l_{R1} = 1$ and $l_{R2} = 1$) are symmetrical as α_p increases from −90° to 90° at an interval of 5°. In terms of the +1st diffraction order, similar experiment results are obtained, as shown in **Figure 4B**. As the ellipticity of the polarized diffraction light from OPHG ($l_{R1} = 1$) increases or decreases, the ellipticity of the same

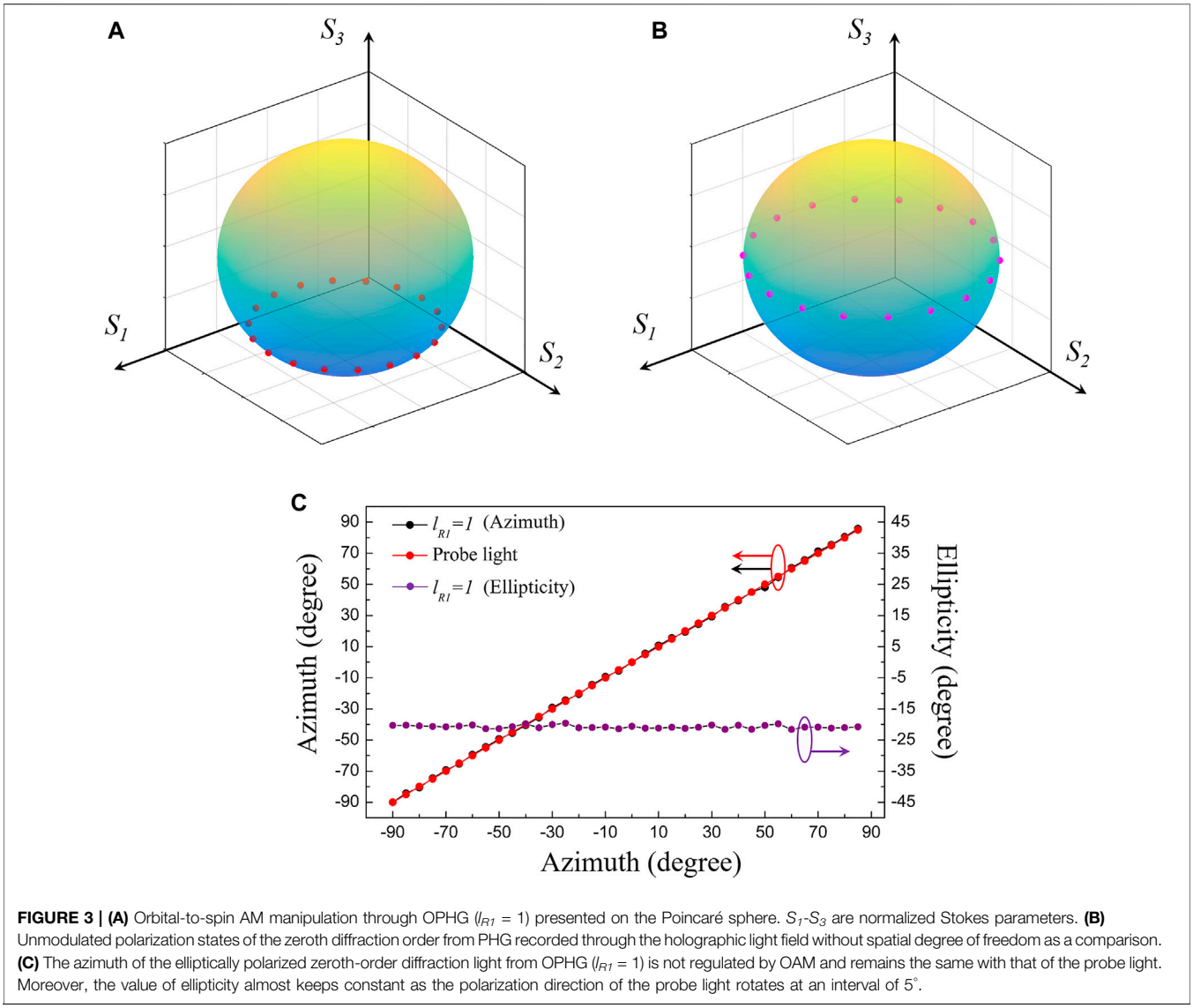

FIGURE 3 | (A) Orbital-to-spin AM manipulation through OPHG (l_{R1} = 1) presented on the Poincaré sphere. S_1-S_3 are normalized Stokes parameters. **(B)** Unmodulated polarization states of the zeroth diffraction order from PHG recorded through the holographic light field without spatial degree of freedom as a comparison. **(C)** The azimuth of the elliptically polarized zeroth-order diffraction light from OPHG (l_{R1} = 1) is not regulated by OAM and remains the same with that of the probe light. Moreover, the value of ellipticity almost keeps constant as the polarization direction of the probe light rotates at an interval of 5°.

diffraction order from OPHG (l_{R2} = 1) goes through the reverse process. Moreover, the symmetrical variation behavior also occurs to the azimuth of the polarization ellipse, as presented in **Figures 4C,D**. With the polarization direction of the probe light rotating, the azimuth of the same diffraction order from the two OPHGs varies conversely.

After reversing the handedness of SAM within the orbital polarization holographic recording field in the previous section, we investigate the effect of spatial degree of freedom of light on polarization manipulation. Similar to OPHGs (l_{R1} = 1 and l_{R2} = 1), ±1st order diffraction beams from OPHGs are detected as OAM increases and the diffraction efficiency is listed as: 7.53% (l_{R1} = 2), 13.47% (l_{R2} = 2), 5.36% (l_{R1} = 3), 13.18% (l_{R2} = 3), 3.08% (l_{R1} = 4) and 10.82% (l_{R2} = 4). Firstly, the ellipticity of the ±1st order diffraction light from the recorded OPHGs is measured and the results are presented in **Figure 5**. In terms of OPHGs (l_{R1} = 2 and l_{R2} = 2) in **Figures 5A,B**, the ellipticity of the same diffraction order is still manipulated symmetrically due to the handedness change of the SAM in the spin-orbital interference field. However, as the effect of OAM continues to be enhanced, the symmetry is broken and the changing behaviors of ellipticity of the 1st order diffraction beams from OPHGs (l_{R1} = 3 and l_{R2} = 3) (**Figures 5C,D**) and OPHGs (l_{R1} = 4 and l_{R2} = 4) (**Figures 5E,F**) tend to be controlled synchronously. For example, in terms of the +1st order diffraction beams from OPHG (l_{R1} = 4) and OPHG (l_{R2} = 4) in **Figure 5F**, the ellipticity of both diffraction beams start to decrease first, then becomes larger, and decrease again in one period. On the other hand, the ellipticity of the zeroth-order diffraction light almost keeps constant and the measurements are listed as: ($-11.13^{\circ} \leq \varepsilon \leq -9.46^{\circ}$) for OPHG ($l_{R1}$ = 2), ($-7.49^{\circ} \leq \varepsilon \leq -5.16^{\circ}$) for OPHG ($l_{R1}$ = 3), ($-14.64^{\circ} \leq \varepsilon \leq -12.15^{\circ}$) for OPHG ($l_{R1}$ = 4), ($-6.24^{\circ} \leq \varepsilon \leq -4.57^{\circ}$) for OPHG ($l_{R2}$ = 2), ($12.26^{\circ} \leq \varepsilon \leq 14.73^{\circ}$) for OPHG ($l_{R2}$ = 3) and ($5.19^{\circ} \leq \varepsilon \leq 7.41^{\circ}$) for OPHG ($l_{R2}$ = 4). Then, we focus on the situation that SPPs with different TCs are fixed in R_1 optical path, as shown in **Figures 5G,H**. Taking the +1st diffraction order from OPHGs (l_{R1} = 1–4) as an example (*see* **Figure 5H**), the ellipticity

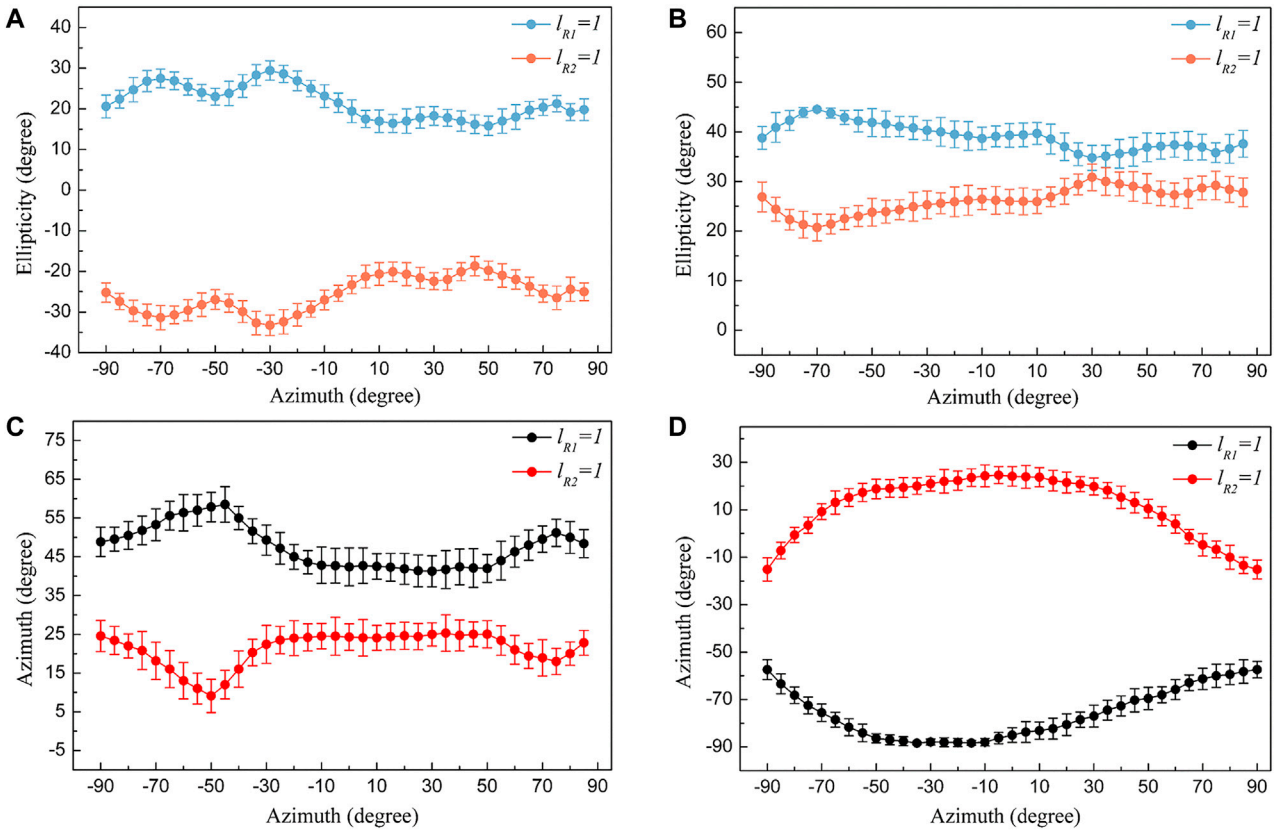

FIGURE 4 | Polarization manipulation through orbital polarization holography when TC = 1. Symmetrical ellipticity control of the -1^{st} **(A)** and $+1^{st}$ **(B)** diffraction orders from OPHGs (l_{R1} = 1 and l_{R2} = 1) with the polarization direction of the probe light being modulated from −90° to 90° at an interval of 5°. Similar to the ellipticity, the azimuth of the -1^{st} **(C)** and $+1^{st}$ order **(D)** polarized diffraction light from the two OPHGs is controlled to change conversely.

decreases first and then keeps an upward tendency with TC increasing from 1 to 4, regardless of the polarization direction of the probe light. Similarly, the ellipticity of the diffraction light from OPHGs (l_{R2} = 1–4) is also controlled by OAM to vary synchronously.

In addition to ellipticity, the azimuth of the $\pm1^{st}$ diffraction order is also modulated by OPHGs, as shown in **Figure 6**. Analogue to the orbit-controlled ellipticity in **Figures 5G,H**, the azimuth of diffraction light also tends to be regulated synchronously by OAM when the SPPs are fixed in one optical path. **Figures 6A,B** report the changing behaviors of azimuth of the $\pm1^{st}$ order diffraction light from OPHGs (l_{R1} = 1–4), respectively. The values of azimuth all go through the increasing-decreasing-increasing processes as TC rises from 1 to 4, whatever the polarization direction of the probe light is. In contrast, for the zeroth diffraction order, the azimuth increases with that of the probe light and there is no obvious difference under four TC conditions, as shown in **Figure 6C**. On the other hand, OAM-controlled azimuth modulation also occurs to the 1^{st} diffraction order of OPHGs (l_{R2} = 1–4). When TC = 2 in **Figures 6D,E**, the azimuth of the $\pm1^{st}$ order diffraction light from OPHGs (l_{R1} = 2 and l_{R2} = 2) is still modulated to change symmetrically. In terms of the $\pm1^{st}$ order diffraction light from OPHGs (l_{R1} = 3 and l_{R2} = 3) in **Figures 6F,G**, the symmetry no longer holds and the variation of azimuth tends to be consistent because of the variation of spin-orbit interaction within the recording light field, where the effect of OAM on the polarization state of the diffraction light is enhanced. Similar results can also be obtained for OPHGs (l_{R1} = 4 and l_{R2} = 4) in **Figure 6H**. In this section, the effect of spatial degree of freedom of light on polarization manipulation is demonstrated experimentally by means of orbital polarization holography.

Jones Matrix Discussion

Orbital polarization holography in photo-alignment liquid crystals is attributed to the interaction between the optical torques induced by SAM (τ_S) and OAM (τ_O) which leads to molecular reorientation, resulting in the formation of a kind of AM-induced birefringence in the sample. Firstly, in terms of the effect of SAM on molecular reorientation, the absorption probability of the *trans*-isomers of liquid crystals is proportional to N [30]

$$N = \langle (\boldsymbol{P} \cdot \boldsymbol{M}(LQ))^2 \rangle = M(LQ) \langle \cos^2 \theta \rangle \quad (1)$$

With < > representing the statistical average, P being the unit vector of the polarization of the interference light field, $M(LQ)$ being the electric dipole transition moment of liquid crystals and θ being the angle between P and $M(LQ)$. According to **Eq. 1**, when N is not equal to 0, liquid crystals will absorb pump light and tend

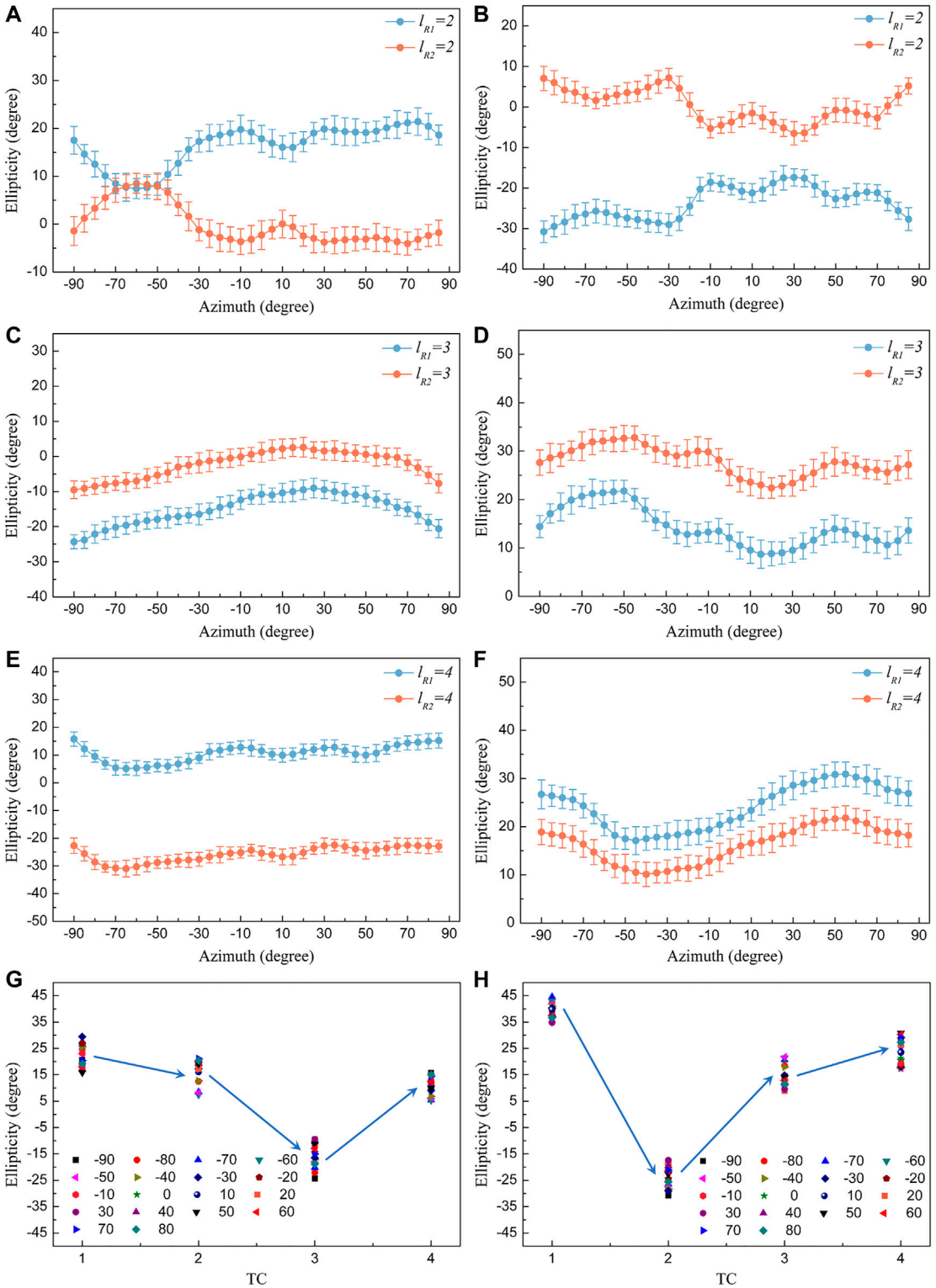

FIGURE 5 | Under the effect of the spatial degree of freedom of recording light on polarization manipulation, the ellipticity of the **(A)** -1^{st} and **(B)** $+1^{st}$ order diffraction light from OPHG ($l_{R1} = 2$) and OPHG ($l_{R2} = 2$) is regulated symmetrically when α_p changes from −90° to 90° at an interval of 5°. With TC increasing, the ellipticity symmetry breaking occurs and the ellipticity of the **(C)** -1^{st} and **(D)** $+1^{st}$ diffraction orders from OPHGs ($l_{R1} = 3$ and $l_{R2} = 3$) varies in a similar trend. Synchronous ellipticity modulation of the **(E)** -1^{st} and **(F)** $+1^{st}$ order diffraction beams from OPHG ($l_{R1} = 4$) and OPHG ($l_{R2} = 4$). OAM-controlled ellipticity variation of the **(G)** -1^{st} and **(H)** $+1^{st}$ diffraction orders from OPHGs (l_{R1} = 1–4) as TC increases from 1 to 4.

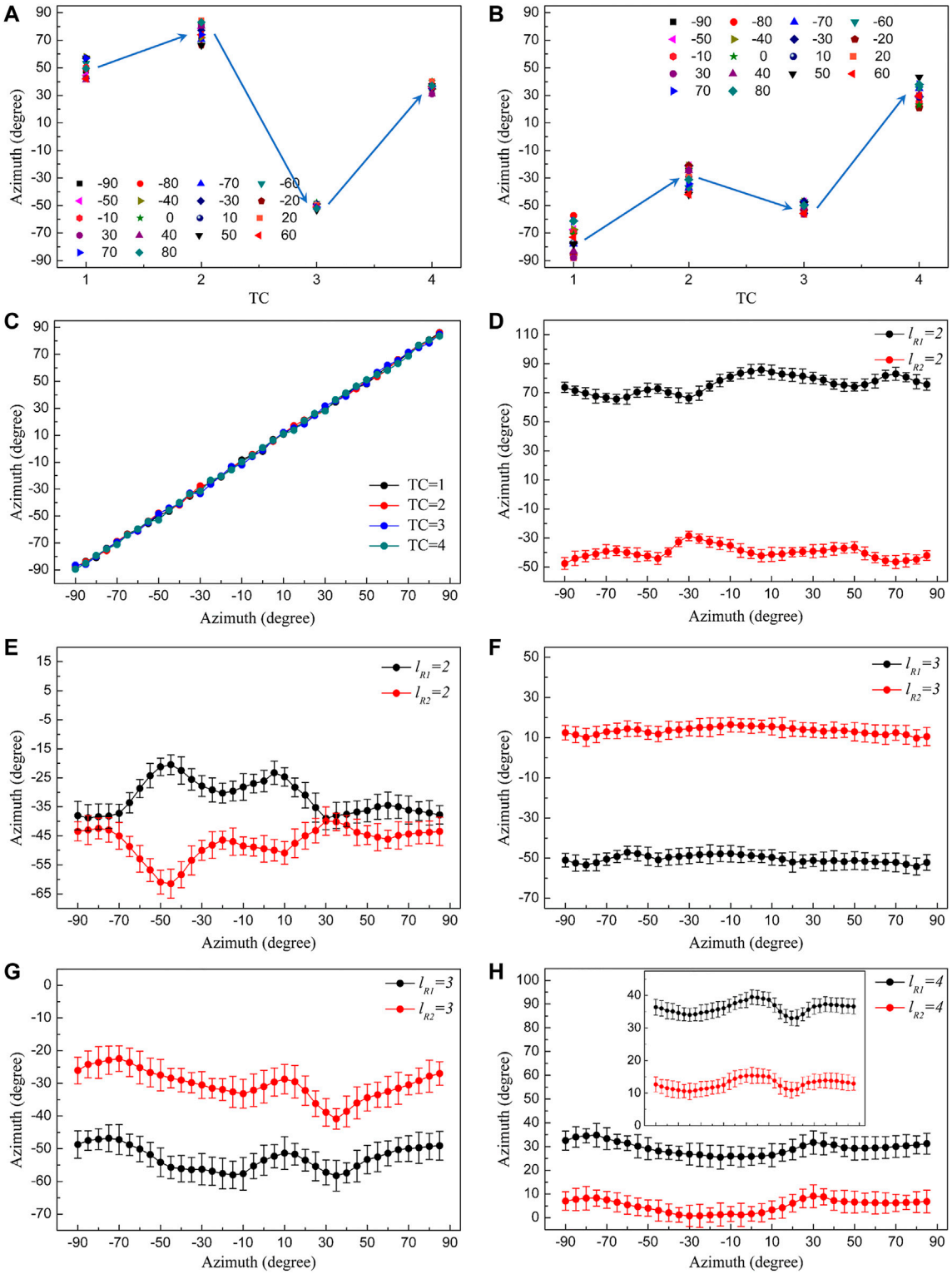

FIGURE 6 | OAM-controlled azimuth variation of the **(A)** -1^{st} and **(B)** $+1^{st}$ diffraction orders from OPHGs (l_{R1} = 1–4) as TC of the vortex recording light increases from 1 to 4. **(C)** The azimuth of the zeroth-order diffraction light is not modulated by OPHGs, regardless of the value of TC. When TC = 2, the azimuth of the **(D)** -1^{st} and **(E)** $+1^{st}$ order diffraction light from OPHGs (l_{R1} = 2 and l_{R2} = 2) is controlled to vary symmetrically. With TC continuing to increase, the effect of OAM is enhanced and the azimuth of the **(F)** -1^{st} and **(G)** $+1^{st}$ diffraction order from OPHGs (l_{R1} = 3 and l_{R2} = 3) tends to vary synchronously. **(H)** Similar azimuth modulation of the $+1^{st}$ diffraction order enabled by spin-orbit coupling when TC = 4. Inset: azimuth of the -1^{st} order diffraction light from OPHGs (l_{R1} = 4 and l_{R2} = 4).

to be reoriented under the force of τ_S. During this process, reversible *trans-cis-trans* photoinduced isomerizations of liquid crystals take place under the action of polarized light. Due to the angular-selective character of light absorption, liquid crystals become uniaxially oriented in a plane perpendicular to the polarization direction of incident light after numerous repetitive isomerization cycles [15]. By virtue of the τ_S-induced reorientation process, SAM-induced birefringence Δn_{SAM} is formed in the sample. Because the polarization direction within the RCP-LCP interference field varies periodically, Δn_{SAM} changes regularly with P. On the other hand, when the polarized light field contains OAM, the orientation of liquid crystals is also forced by an OAM-induced torque τ_O that is in the azimuthal direction of OAM [31]. Under the effect of OAM, τ_O-induced deflection of molecular reorientation occurs and the liquid crystals are no longer perpendicular to the polarization direction, which exerts an influence on the SAM-induced birefringence. Thus, molecular rearrangement within the orbital polarization holographic recording field is based on τ_S and affected by τ_O, leading to the formation of a kind of AM-induced birefringence Δn_{AM}. The periodically distributed AM-induced birefringence generated through spin-orbit coupling is contributed to the formation of OPHG and its diffraction properties.

Based on the discussion above, the value of Δn_{AM} is calculated to interpret OAM-enabled polarization manipulation. We start from the transmission matrix of OPHG. Let us consider the Jones matrix of a general anisotropic element

$$\boldsymbol{T_a}(0) = \begin{pmatrix} e^{i\frac{\Delta\varphi}{2}} & 0 \\ 0 & e^{-i\frac{\Delta\varphi}{2}} \end{pmatrix} \tag{2}$$

The anisotropic phase retardation is $\Delta\varphi = 2\pi\Delta n d/\lambda_p$ with Δn being the photoinduced birefringence, λ_p being the wavelength of probe light and d being the thickness of the sample. When the anisotropy axis is oriented at an angle of γ in x-y plane (*see* **Figure 1A**), the transmission matrix turns to

$$\boldsymbol{T_a}(\gamma) = \boldsymbol{R}(-\gamma)\cdot\boldsymbol{T_a}(0)\cdot\boldsymbol{R}(\gamma) \tag{3}$$

Where the rotation matrix is $\boldsymbol{R}(\gamma) = \begin{pmatrix} \cos\gamma & -\sin\gamma \\ \sin\gamma & \cos\gamma \end{pmatrix}$. In terms of PHG, $\Delta\varphi$ is only induced by SAM ($\Delta\varphi_{SAM}$) and the anisotropy-axis orientation varies periodically in x-direction, expressed as $\gamma = \gamma_0 + \gamma(x)$. From **Eq. 3**, $\boldsymbol{T}_{\mathrm{a}}^{\mathrm{SAM}} = \boldsymbol{T_0^{SAM}} + \boldsymbol{T_{\pm 1}^{SAM}}$ and the 1st order transmission matrix of PHG is

$$\boldsymbol{T_{\pm 1}^{SAM}} = \frac{i\exp(\pm 2i\gamma)}{2}\sin\left(\frac{\Delta\varphi_{SAM}}{2}\right)\begin{pmatrix} 1 & \pm i \\ \pm i & -1 \end{pmatrix} \tag{4}$$

The polarization state of the 1st order diffraction light is calculated as

$$\boldsymbol{E_{\pm 1}} = \boldsymbol{T_{\pm 1}^{SAM}}\cdot\boldsymbol{R_P} = \boldsymbol{T_{\pm 1}^{SAM}}\cdot\begin{pmatrix} \cos\alpha_p \\ \sin\alpha_p \end{pmatrix} \tag{5}$$

$$\boldsymbol{E_{\pm 1}} = \frac{i\exp(\pm 2i\gamma)\exp(\pm i\alpha_p)}{2}\sin\left(\frac{\Delta\varphi_{SAM}}{2}\right)\begin{pmatrix} 1 \\ \pm i \end{pmatrix} \tag{6}$$

Where R_P represents the Jones vector of the linearly polarized probe light. According to **Eq. 6**, the LCP and RCP components of the probe light are divided and converted into RCP and LCP, respectively.

In terms of OPHG, SAM-induced molecular reorientation is affected by τ_O and OAM-induced birefringence is formed within the recording area. In this case, $\Delta\varphi_{AM} = 2\pi\Delta n_{AM} d/\lambda_p$ is formed through SAM-OAM coupling. According to **Eq. 3**, the transmission matrix of OPHG can be expressed as [21].

$$\boldsymbol{T_a^{SAM-OAM}} = \begin{pmatrix} \cos\left(\frac{\Delta\varphi_{AM}}{2}\right) & i\sin\left(\frac{\Delta\varphi_{AM}}{2}\right)e^{-2i\gamma} \\ i\sin\left(\frac{\Delta\varphi_{AM}}{2}\right)e^{2i\gamma} & \cos\left(\frac{\Delta\varphi_{AM}}{2}\right) \end{pmatrix} \tag{7}$$

In order to calculate the value of Δn_{AM}, we start from the zeroth-order transmission matrix

$$\sqrt{\eta_0}e^{i\delta_0}\begin{pmatrix} \cos\alpha_0\cos\varepsilon_0 - i\sin\alpha_0\sin\varepsilon_0 \\ \sin\alpha_0\cos\varepsilon_0 + i\cos\alpha_0\sin\varepsilon_0 \end{pmatrix} = \boldsymbol{T_0^{SAM-OAM}}\begin{pmatrix} \cos\alpha_p \\ \sin\alpha_p \end{pmatrix} \tag{8}$$

With δ_0 and η_0 being the phase and diffraction efficiency of the zeroth diffraction order, respectively. Based on the experimental results, the azimuth of the zeroth-order diffraction light α_0 is not modulated by OPHG and we obtain

$$\boldsymbol{T_0^{SAM-OAM}} = \sqrt{\eta_0}e^{i\delta_0}\begin{pmatrix} \cos\varepsilon_0 & -i\sin\varepsilon_0 \\ i\sin\varepsilon_0 & \cos\varepsilon_0 \end{pmatrix} \tag{9}$$

With ε_0 being the ellipticity of the zeroth-order diffraction light. Then, AM-induced birefringence Δn_{AM} can be calculated as follows

$$\boldsymbol{E_{\pm 1}} = \begin{pmatrix} E_{\pm 1x} \\ E_{\pm 1y} \end{pmatrix} = \sqrt{\eta_{\pm 1}}e^{i\delta_{\pm 1}}\begin{pmatrix} \cos\alpha_{\pm 1}\cos\varepsilon_{\pm 1} - i\sin\alpha_{\pm 1}\sin\varepsilon_{\pm 1} \\ \sin\alpha_{\pm 1}\cos\varepsilon_{\pm 1} + i\cos\alpha_{\pm 1}\sin\varepsilon_{\pm 1} \end{pmatrix} \tag{10}$$

In which $\alpha_{\pm 1}$, $\varepsilon_{\pm 1}$, $\delta_{\pm 1}$ and $\eta_{\pm 1}$ represent the azimuth, ellipticity, phase and diffraction efficiency of the $\pm 1^{\mathrm{st}}$ order diffraction light, respectively. According to **Eqs 7**, **9**, **10**, the equation of Δn_{AM} is

$$\sin\left(\frac{\Delta\varphi_{AM}}{2}\right) = \frac{\sqrt{\eta_0}e^{i\delta_0}\sin\varepsilon_0 + i\left[(E_{+1x} + E_{-1x})\sin\alpha_p - (E_{+1y} + E_{-1y})\cos\alpha_p\right]}{e^{2i\gamma} - 2\cos(2\gamma)\sin^2\alpha_p} \tag{11}$$

Similar to the SAM condition, the phases of the $\pm 1^{\mathrm{st}}$ order diffraction light are the functions of γ and α_p. Based on the experimental data, the plural numerator is proportional to the plural denominator in **Eq. 11** and the ratio is a real number. The values of Δn_{AM} under our experimental conditions are calculated to equal 0.068 (Δn_{SAM}), 0.063 ($l_{R1} = 1$), 0.072 ($l_{R2} = 1$), 0.055 ($l_{R1} = 2$), 0.074 ($l_{R2} = 2$), 0.046 ($l_{R1} = 3$), 0.073 ($l_{R2} = 3$), 0.035 ($l_{R1} = 4$), 0.066 ($l_{R2} = 4$),

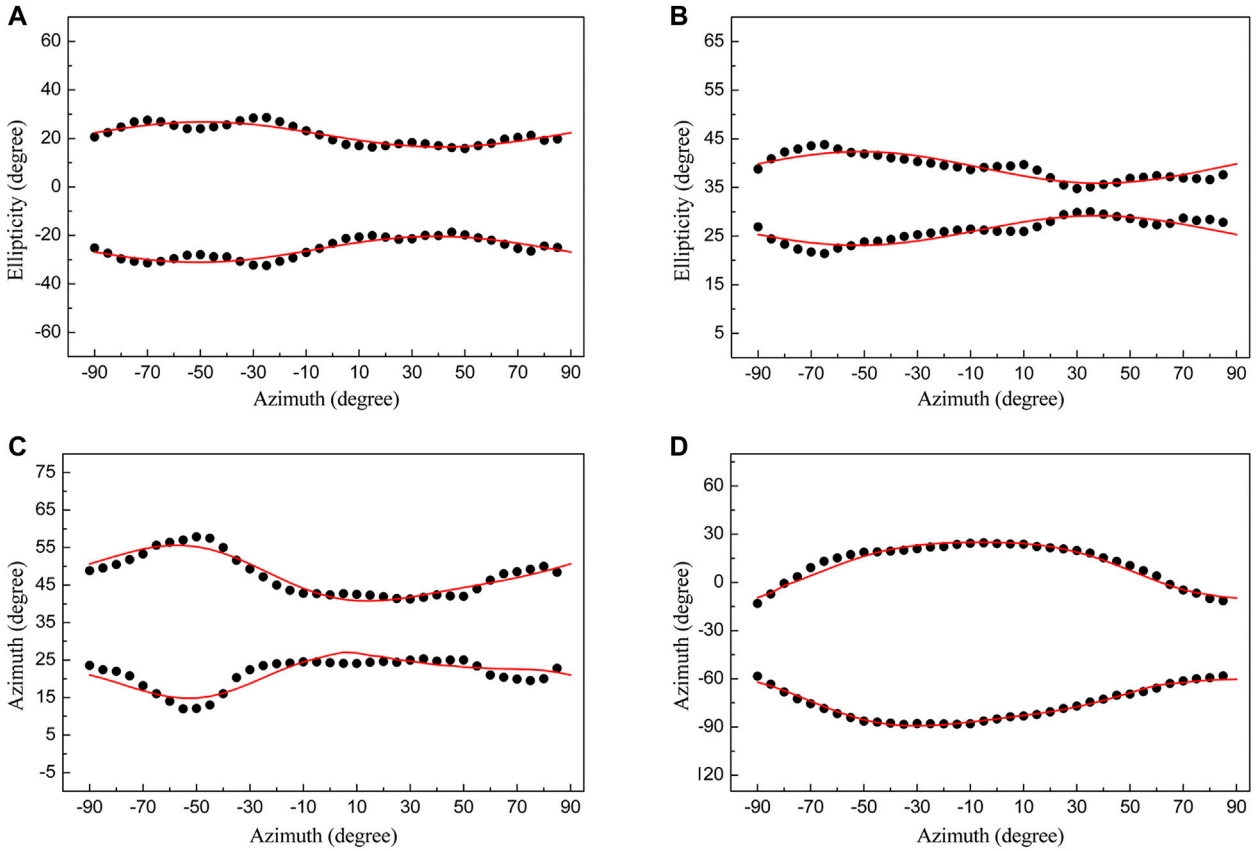

FIGURE 7 | Simulated curves and experimental data of orbital polarization holographic manipulation in terms of OPHGs (l_{R1} = 1 and l_{R2} = 1). **Figures 7A–D** and **Figures 4A–D** are in one-to-one correspondence. There is an agreement between the theoretical analysis and experimental results.

respectively. Taking OPHGs ($l_{R1} = 1$ and $l_{R2} = 1$) as examples, theoretical simulations of orbital polarization holographic manipulation are presented in **Figure 7**, and there is a good agreement between the theoretical analysis and experimental results. Moreover, it can be noticed that Δn_{AM} is always smaller than Δn_{SAM} and continues to be attenuated when l_{R1} increases from 1 to 4. In contrast, the value of Δn_{AM} increases with the enhancement of OAM carried by R_2 recording light at first, while starts to decrease when $l_{R2} \geq 3$. The reason is that, when SPPs are placed in the optical path of R_1, the effect of OAM weakens the component of SAM-induced birefringence in the sample during the process of spin-orbit coupling. On the other hand, when TC increases, the size of singularity of the vortex recording beam becomes larger and the light intensity within the spatially limited interference area decreases. Under the combined weakening effects of OAM and light intensity, Δn_{AM} decreases significantly from 0.068 to 0.035 when l_{R1} rises to 4. When R_2 becomes the vortex light, SAM handedness of the interference field is reversed and the SAM-induced birefringence is enhanced by OAM, leading to the increase of Δn_{AM}. In the case of $l_{R2} = 3$ and 4, though the value of TC becomes larger, the weakening effect of light intensity is greater than the enhancing effect of OAM, leading to the decrease of Δn_{AM}. In this section, the mechanism of polarization manipulation enabled through orbital polarization holography has been explained theoretically.

DISCUSSION

In conclusion, all-optical polarization manipulation through orbital polarization holography has been demonstrated experimentally and analyzed theoretically with Jones matrices. The polarization states of diffraction light from the recorded OPHGs are able to be controlled regularly under the effect of spatial degree of freedom of recording light because of optical SAM-OAM coupling during the process of light-matter interactions, resulting in the formation of a kind of periodically distributed AM-induced birefringence structure in photo-alignment liquid crystals. Furthermore, the transmission matrix of OPHGs and the value of AM-induced birefringence are

calculated with Jones matrices in order to interpret the mechanism of orbit-controlled polarization manipulation. Based on the previous research on SAM-to-OAM conversion, orbit-induced polarization modulation is realized in this work, which may enrich the field of optical manipulation.

DATA AVAILABILITY STATEMENT

The original contributions presented in the study are included in the article/Supplementary Material, further inquiries can be directed to the corresponding author.

AUTHOR CONTRIBUTIONS

ZL: performed the experiments, processed and analysed the data, and wrote the article; CW: performed part of the experiments, reviewed the paper and provided technical assistance. All authors approved the final version of the article.

FUNDING

This work is supported by National Natural Science Foundation of China (NSFC) (grant 92050116).

REFERENCES

1. Perreault WE, Zhou H, Mukherjee N, Zare RN. A Bi-axial Quantum State that Controls Molecular Collisions like a Double-Slit Interferometer. *Front Phys* (2021) 9:671997. doi:10.3389/fphy.2021.671997
2. Bandrauk AD, Chelkowski S, Yuan K-J. Electronic Currents and Magnetic Fields in H2+ Induced by Coherent Resonant Bichromatic Circularly Polarized Laser Pulses: Effects of Orientation, Phase, and Helicity. *Front Phys* (2021) 9: 675375. doi:10.3389/fphy.2021.675375
3. Bekshaev A, Vasnetsov M. Vortex Flow of Light: "Spin" and "Orbital" Flows in a Circularly Polarized Paraxial Beam. In: *Twisted Photons: Applications of Light with Orbital Angular Momentum*. Weinheim: Wiley-VCH Verlag GmbH & Co. KGaA (2011). p. 13–24. doi:10.1002/9783527635368.ch2
4. Xiao W, Chen Y, Han K, Shen X, Wang W. Tailoring Spin Angular Momentum of Light: Design Principles for Plasmonic Nanostructures. *Phys Rev Appl* (2020) 13:014029. doi:10.1103/physrevapplied.13.014029
5. de Aguiar HB, Gigan S, Brasselet S. Polarization Recovery through Scattering media. *Sci Adv* (2017) 3:e1600743. doi:10.1126/sciadv.1600743
6. Nicholls LH, Rodríguez-Fortuño FJ, Nasir ME, Córdova-Castro RM, Olivier N, Wurtz GA, et al. Ultrafast Synthesis and Switching of Light Polarization in Nonlinear Anisotropic Metamaterials. *Nat Photon* (2017) 11:628–33. doi:10.1038/s41566-017-0002-6
7. Plutenko DO, Vasnetsov MV. Scattering of the Radial Polarized Beams on the Metal Spherical Particle: Plasmonic Nanojet Formation. *Front Phys* (2021) 9: 727525. doi:10.3389/fphy.2021.727525
8. Sarmiento-Merenguel JD, Halir R, Le Roux X, Alonso-Ramos C, Vivien L, Cheben P, et al. Demonstration of Integrated Polarization Control with a 40 dB Range in Extinction Ratio. *Optica* (2015) 2:1019–23. doi:10.1364/optica.2.001019
9. Li X, Zhou Y, Cai Y, Zhang Y, Yan S, Li M, et al. Generation of Hybrid Optical Trap Array by Holographic Optical Tweezers. *Front Phys* (2021) 9:591747. doi:10.3389/fphy.2021.591747
10. Zhang Z, Qiao X, Midya B, Liu K, Sun J, Wu T, et al. Tunable Topological Charge Vortex Microlaser. *Science* (2020) 368:760–3. doi:10.1126/science.aba8996
11. Puentes G, Banerji A. Generation of High-Order Vortex States from Two-Mode Squeezed States. *Front Phys* (2021) 9:690721. doi:10.3389/fphy.2021.690721
12. Oemrawsingh SSR, van Houwelingen JAW, Eliel ER, Woerdman JP, Verstegen EJK, Kloosterboer JG, et al. Production and Characterization of Spiral Phase Plates for Optical Wavelengths. *Appl Opt* (2004) 43:688–94. doi:10.1364/ao.43.000688
13. Ren H, Briere G, Fang X, Ni P, Sawant R, Héron S, et al. Metasurface Orbital Angular Momentum Holography. *Nat Commun* (2019) 10:2986. doi:10.1038/s41467-019-11030-1
14. Fang X, Ren H, Gu M. Orbital Angular Momentum Holography for High-Security Encryption. *Nat Photon* (2020) 14:102–8. doi:10.1038/s41566-019-0560-x
15. Ryabchun A, Sakhno O, Stumpe J, Bobrovsky A. Full-Polymer Cholesteric Composites for Transmission and Reflection Holographic Gratings. *Adv Opt Mater* (2017) 5:1700314. doi:10.1002/adom.201700314
16. Callegari F, Le Gratiet A, Zunino A, Mohebi A, Bianchini P, Diaspro A. Polarization Label-free Microscopy Imaging of Biological Samples by Exploiting the Zeeman Laser Emission. *Front Phys* (2021) 9:758880. doi:10.3389/fphy.2021.758880
17. Cazac V, Achimova E, Abashkin V, Prisacar A, Loshmanschii C, Meshalkin A, et al. Polarization Holographic Recording of Vortex Diffractive Optical Elements on Azopolymer Thin Films and 3D Analysis via Phase-Shifting Digital Holographic Microscopy. *Opt Express* (2021) 29:9217–30. doi:10.1364/oe.415639
18. Zang J, Kang G, Li P, Liu Y, Fan F, Hong Y, et al. Dual-channel Recording Based on the Null Reconstruction Effect of Orthogonal Linear Polarization Holography. *Opt Lett* (2017) 42:1377–80. doi:10.1364/ol.42.001377
19. Shen Y, Wang X, Xie Z, Min C, Fu X, Liu Q, et al. Optical Vortices 30 Years on: OAM Manipulation from Topological Charge to Multiple Singularities. *Light Sci Appl* (2019) 8:90. doi:10.1038/s41377-019-0194-2
20. Lyu Z, Wang C. All-optically Phase-Induced Polarization Modulation by Means of Holographic Method. *Sci Rep* (2020) 10:5657. doi:10.1038/s41598-020-62549-z
21. Bliokh KY, Rodríguez-Fortuño FJ, Nori F, Zayats AV. Spin-orbit Interactions of Light. *Nat Photon* (2015) 9:796–808. doi:10.1038/nphoton.2015.201
22. Georgi P, Schlickriede C, Li G, Zhang S, Zentgraf T. Rotational Doppler Shift Induced by Spin-Orbit Coupling of Light at Spinning Metasurfaces. *Optica* (2017) 4:1000–5. doi:10.1364/optica.4.001000
23. Devlin RC, Ambrosio A, Rubin NA, Mueller JPB, Capasso F. Arbitrary Spin-To-Orbital Angular Momentum Conversion of Light. *Science* (2017) 358: 896–901. doi:10.1126/science.aao5392
24. Arzola AV, Chvátal L, Jákl P, Zemánek P. Spin to Orbital Light Momentum Conversion Visualized by Particle Trajectory. *Sci Rep* (2019) 9:4127. doi:10.1038/s41598-019-40475-z
25. Zhao Y, Edgar JS, Jeffries GD, McGloin D, Chiu DT. Spin-to-Orbital Angular Momentum Conversion in a Strongly Focused Optical Beam. *Phys Rev Lett* (2007) 99:073901. doi:10.1103/PhysRevLett.99.073901
26. Saito S. Poincaré Rotator for Vortexed Photons. *Front Phys* (2021) 9:646228. doi:10.3389/fphy.2021.646228
27. Xiao S, Lu X, Lu Q. Photosensitive Polymer from Ionic Self-Assembly of Azobenzene Dye and Poly(ionic Liquid) and its Alignment Characteristic toward Liquid crystal Molecules. *Macromolecules* (2007) 40:7944–50. doi:10.1021/ma070972s
28. Gregg P, Kristensen P, Rubano A, Golowich S, Marrucci L, Ramachandran S. Enhanced Spin Orbit Interaction of Light in Highly Confining Optical Fibers for Mode Division Multiplexing. *Nat Commun* (2019) 10:4707. doi:10.1038/s41467-019-12401-4
29. Li Y, Kim J, Escuti MJ. Orbital Angular Momentum Generation and Mode Transformation with High Efficiency Using Forked Polarization Gratings. *Appl Opt* (2012) 51:8236–45. doi:10.1364/ao.51.008236
30. Tawa K, Kamada K, Kiyohara K, Ohta K, Yasumatsu D, Sekkat Z, et al. Photoinduced Reorientation of Azo Dyes Bonded to Polyurethane Studied by

Polarized FT-IR Spectroscopy. *Macromolecules* (2001) 34:8232–8. doi:10.1021/ma002009r

31. Yao AM, Padgett MJ. Orbital Angular Momentum: Origins, Behavior and Applications. *Adv Opt Photon* (2011) 3:161–204. doi:10.1364/aop.3.000161

Conflict of Interest: The authors declare that the research was conducted in the absence of any commercial or financial relationships that could be construed as a potential conflict of interest.

Publisher's Note: All claims expressed in this article are solely those of the authors and do not necessarily represent those of their affiliated organizations, or those of the publisher, the editors and the reviewers. Any product that may be evaluated in this article, or claim that may be made by its manufacturer, is not guaranteed or endorsed by the publisher.